Theoretical study of electrorheological behavior of a nematic liquid crystal confined by two cylindrical surfaces with different anchoring energies

G. Rivas⬤ and J. A. Reyes

Instituto de Física, Universidad Nacional Autónoma de México, Apartado Postal 20-364 01000, Ciudad de México, México

D. Martínez⬤*

Universidad Autónoma de la Ciudad de México, Campus Cuautepec, Av. La Corona 320, Col. Loma la Palma, Alcaldía Gustavo A. Madero, 07160, Ciudad de México, México

Electrorheological response of a nematic liquid crystal confined in the region between two coaxial and rotating circular cylinders is studied theoretically. Utilizing weak anchoring conditions, the physical properties of 4-n-pentyl-4-cyanobiphenyl (5CB), nonslip boundary conditions, and contrasting surface anchoring energies, we numerically obtain the equilibrium configurations for the nematic director under the influence of an external low-frequency radial electric field and the corresponding (angular) velocity profiles. The Fréedericksz transition is parametrized by the cylinders' radii ratio for different values of the surface energies. The averaged apparent viscosity of the nematic is calculated also.

I. INTRODUCTION

Since their discovery in 1888 [1], liquid crystals (LCs) have received increasing interest from the scientific community because of their wide variety of technological applications, such as liquid crystal displays [2], electro-optical devices [3], wavelength filters [4], and liquid crystal thermometers [5].

Systems involving liquid crystals confined between two concentric cylinders have been investigated to elucidate their flow [6], the Fréedericksz transition occurring in the absence of external electric field [7], and their flexoelectric instability [8] by applying a stability analysis based on the orientational profile [9]. These studies were motivated by the original problem proposed by Meyer, solved in a special case by Parodi, and then discussed in the book of de Gennes [10]. Subsequently, the same problem was reexamined by Williams [11] by considering that the elastic constants of splay and bend are different, in the strong anchoring approximation. Very recently, the equilibrium problem for a nematic liquid crystal confined within two parallel eccentric cylinders with homeotropic anchoring on the lateral boundaries has been rigorously analyzed by Rosso *et al.* [12] in the framework of a purely director approach.

However, electrorheological fluids (ERFs), which consist of polarizable particles immersed in a nonpolarizable solvent from which fibrillated structures are formed when external electric fields are applied, have been widely used. Contrary to traditional LCs where agglomeration and sedimentation of particles and erosion issues are constantly found [13], ERFs are highly homogeneous due to the absence of suspended particles which has encouraged its application to

microsystems [14]. Also, apparent viscosity of ERFs is controlled by external electric fields. In 2002, Yoshida *et al.* [15] studied the properties of ERFs to manipulate the flow through micro valves.

Yang *et al.* [16] demonstrate the ability of a LC to function as an ERF and also that the viscosity of a polymeric liquid crystal increased an order of magnitude after the application of an external field. In the work of Volder *et al.* [13], a microcapillary tube filled by nematic liquid crystal (NLC) was considered and variations of the flow due to the presence of an external electric field were studied.

Electrorheological response of a confined NLC is strongly influenced by the physical properties of the boundary walls [17,18]. Depending on the methods or techniques used to induced a surface alignment [19,20], anchoring conditions could be strong [21,22] or weak [23,24] and their general properties can be expressed by using the Rapini-Papoular model [25]. Experimentally, there is also a wide range of values for this surface anchoring energy [26,27].

Fréedericksz transition, first discovered in magnetic experiments [28,29], is related to the reorientation of the molecules of the NLC once the external field (electric or magnetic) has reached some threshold value and overcomes the anchoring energies at the confining surfaces and the elastic energy of the bulk [30]. This configurational transition has been widely used in electro-optical devices [31].

In this paper we study the response of the 4-n-pentyl-4-cyanobiphenyl (5CB) NLC confined in the region between two coaxial circular cylinders, which rotate at different constant angular velocities and where a low-frequency (KHz) radial electric field is applied. By considering no-slip boundary conditions and weak anchoring conditions, in Sec. II we establish the total energy density, and use variational methods to derive the equilibrium equations satisfied by the director at
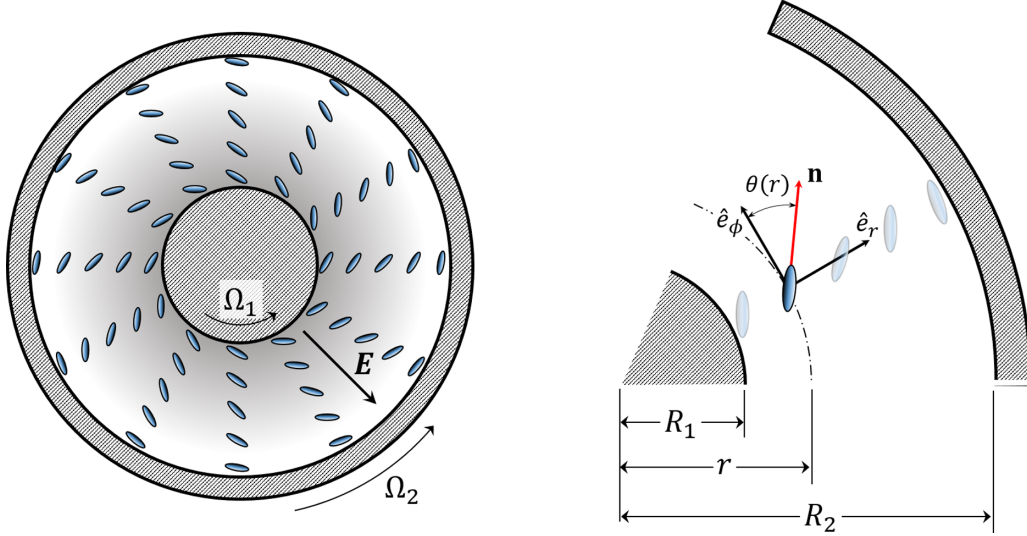
———
*dmartinezs77@yahoo.com.mx

FIG. 1. Longitudinal section of the coaxial circular cylinders. A nematic liquid crystal between two coaxial cylinders which rotate at different angular velocities Ω_1 and Ω_2. Also, the radial AC electric field applied to the nematic and the angle of inclination $\theta(r)$ of the director $\mathbf{n} = \sin\theta(r)\hat{\mathbf{e}}_r + \cos\theta(r)\hat{\mathbf{e}}_\phi$ are shown.

the cylindrical surfaces. From the nematodynamic theory, we also derive differential equation for the director in the bulk and for the velocity profile. In Sec. III, we solve numerically these equilibrium equations to obtain the director configuration of the NLC, the velocity profile and the threshold field for different values of the surface anchoring energies ratio and parametrized by the cylinders radii ratio and the electric field strength. In Sec. IV, we obtain the averaged apparent viscosity. Finally, in Sec. V we give some concluding remarks.

II. BASIC EQUATIONS

We consider a nematic between two coaxial circular cylinders with radii R_1 and R_2 ($R_1 < R_2$) which rotate at constant angular velocities Ω_1 and Ω_2, respectively (Fig. 1). It is important to mention that the same system and geometry was previously analyzed in Refs. [6,32], but by assuming strong anchoring boundary condition for the nematic director and in the absence of electric field. This problem indeed was already considered by Atkin and Leslie [6] many years ago where a similar notation to the one we use here was employed.

Under the action of a low-frequency electric field, the director is spatially homogeneous along the axis of the tubes. Thus, in cylindrical coordinates $(x_1, x_2, x_3) = (r, \phi, z)$, we express the director and the velocity field as

$$\mathbf{n} = \sin\theta(r)\hat{\mathbf{e}}_r + \cos\theta(r)\hat{\mathbf{e}}_\phi \tag{1}$$

and

$$\mathbf{v} = v_\phi\hat{\mathbf{e}}_\phi \equiv r\omega(r)\hat{\mathbf{e}}_\phi, \tag{2}$$

where $\theta(r)$ is the orientational angle measured from the ϕ axis and $\hat{\mathbf{e}}_r$ and $\hat{\mathbf{e}}_\phi$ are the unitary vectors along the radial and the azimuthal direction, respectively. Also, we assume the no-slip boundary conditions

$$\omega(r = R_1) = \Omega_1, \quad \omega(r = R_2) = \Omega_2. \tag{3}$$

For the present physical system, the elastic Frank-Oseen energy density is

$$2F_{fo} = K_1(\nabla \cdot \hat{\mathbf{n}})^2 + K_2(\hat{\mathbf{n}} \cdot \nabla \times \hat{\mathbf{n}})^2 + K_3(\hat{\mathbf{n}} \times \nabla \times \hat{\mathbf{n}})^2$$
$$- K_{24}\nabla \cdot (\mathbf{n}\nabla \cdot \mathbf{n} + \mathbf{n} \times \nabla \times \mathbf{n}), \tag{4}$$

where the elastic moduli K_1, K_2, and K_3 refer to splay, twist, and bend deformations, respectively, while K_{24} is the saddle-splay elastic constant [32,33].

Also, for an applied low-frequency radial electric field between the cylindrical surfaces, $\mathbf{E}(r)$, the electric energy density is given as

$$F_{\text{elec}} = -\frac{1}{2}\mathbf{D} \cdot \mathbf{E} = -\frac{1}{2}\epsilon_{rr}(r)E^2, \tag{5}$$

where $\mathbf{D}$ is the electric displacement and $\epsilon_{rr}(r)$ is an element of the dielectric tensor ϵ_{ij}. Since we are dealing with an uniaxial nematic, the dielectric tensor is expressed as [34]

$$\epsilon_{ij} = \epsilon_\perp\delta_{ij} + \epsilon_a n_i n_j, \tag{6}$$

with $\epsilon_a = \epsilon_\parallel - \epsilon_\perp$ the dielectric anisotropy, and $\epsilon_\parallel$ and $\epsilon_\perp$ the parallel and perpendicular dielectric constants of the nematic, respectively.

Moreover, if $\Delta\Phi$ is the fixed electric potential maintained at the cylinders, then the electric field between the surfaces $r = R_1$ and $r = R_2$ is given as $\mathbf{E}(r) = -\mathbf{u}_r\Delta\Phi/r\ln(R_2/R_1)$. It is worth to mention that this is only a electrostatic solution, so we are assuming a quasistatic approximation to model a low-frequency field in the order of KHz. Hence, from Eqs. (1), (5), and (6), the electric energy density can be written in the following way:

$$F_{\text{elec}} = -\frac{qK_1}{2r^2}\left(\sin^2\theta + \frac{\epsilon_\perp}{\epsilon_a}\right), \tag{7}$$

where the parameter

$$q \equiv \epsilon_a(\Delta\Phi)^2/K_1\ln^2(R_2/R_1) \tag{8}$$

is the ratio of the electric and elastic energies. As can be seen the value q does not depends on the sign of $\Delta\Phi$ so it does not matter which cylinder has the larger voltage. Thus, for $q \ll 1$ the influence of the field is weak, meanwhile for $q \gg 1$ the applied electric field overcomes the molecular elastic forces.

However, the energy density due to the movement of the LC is

$$F_h = \tfrac{1}{2}\rho v^2, \tag{9}$$

where ρ is the mass density of the nematic and $v \equiv |\mathbf{v}|$ is the magnitude of the velocity field.

We obtain the total energy of the nematic by using Eqs. (4), (7), and (9) and by taking into account that the surface energy density of the NLC at each cylindrical surface energy density is modeled by the Rapini-Papoular anchoring potential [25,35]

$$F_s[\theta(R_i)] = \frac{\tau_0}{2}\sin^2(\theta(R_i) - \theta_0), \ i = 1, 2, \tag{10}$$

where θ_0 is the tilt angle [36] and τ_0 is the surface anchoring energy whose values depend on the LC properties at each cylindrical surface.

Therefore, the total free energy for the NLC is expressed as

$$\mathcal{F} = \int_V (F_{fo} + F_{\text{elec}} + F_h)dV + \int_{S_1} F_s[\theta(R_1)]dS_1$$
$$+ \int_{S_2} F_s[\theta(R_2)]dS_2. \tag{11}$$

By performing the change of variable $x = r/R_2$, introducing the parameters $\kappa = K_3/K_1$, $a = R_1/R_2$, expressing $\nabla \cdot \mathbf{n}$ and $\nabla \times \mathbf{n}$ in cylindrical coordinates, and considering that at the cylindrical surfaces the tilt angles satisfy $\theta_0(a) = 0 = \theta_0(1)$, we obtain that the total free energy per unit length, $f \equiv \mathcal{F}/L$ (L the length of the cylinders), can be written in the following form:

$$f = \int_a^1 f_B\left(\theta, \frac{d\theta}{dx}\right)dx + f_S[\theta(a)] + f_S[\theta(1)], \tag{12}$$

with f_B and f_S the bulk and surface functions given as

$$f_B\left(\theta, \frac{d\theta}{dx}\right) = \pi K_1 x(\cos^2\theta + \kappa \sin^2\theta)\left(\frac{d\theta}{dx}\right)^2$$
$$+ \frac{\pi K_1}{x}(\sin^2\theta + \kappa \cos^2\theta)$$
$$- \pi K_1 q x\left(\sin^2\theta + \frac{\epsilon_\perp}{\epsilon_\parallel}\right) + \pi R_2^4 \rho \omega^2 x^3, \tag{13}$$

where

$$f_S[\theta(a)] = \pi K_1 \sigma_a \sin^2\theta(a), \tag{14}$$

$$f_S[\theta(1)] = \pi K_1 \sigma_1 \sin^2\theta(1) \tag{15}$$

are functions defined only at the cylindrical surfaces and

$$\sigma_a \equiv \left(\frac{aR_2}{K_1}\right)\tau_{0_a} + \kappa - 1, \quad \sigma_1 \equiv \left(\frac{R_2}{K_1}\right)\tau_{0_1} - (\kappa - 1), \tag{16}$$

with τ_{0_a} and τ_{0_1} the anchoring energies at inner ($x = a$) and outer ($x = 1$) cylinders, respectively. The dimensionless

parameters σ_a and σ_1 can be considered as ratios between the effective surface anchoring energy at each cylinder and the elastic bulk energy.

To obtain the anchoring conditions satisfied by the director $\mathbf{n}$, the total free energy of the nematic must be minimized. Thus, using a standard variational calculus procedure, we can derive the bulk expression f_B with respect to both θ and $d\theta/dx$, and considering the surface function f_S to obtain that

$$\delta f = \int_a^1 \left[\left(\frac{\partial f_B}{\partial \theta}\right)\delta\theta + \left(\frac{\partial f_B}{\partial(d\theta/dx)}\right)\delta\left(\frac{d\theta}{dx}\right)\right]dx$$
$$+ \left[\left(\frac{d\Phi_S}{dx}\right)\delta\theta(x)\right]_{x=1} + \left[\left(\frac{d\Phi_S}{dx}\right)\delta\theta(x)\right]_{x=a}. \tag{17}$$

Since $\delta(\frac{d\theta}{dx}) = \frac{d}{dx}(\delta\theta)$ and using the identity

$$\frac{d}{dx}\left(\frac{\partial f_B}{\partial(d\theta/dx)}\delta\theta\right)$$
$$= \frac{d}{dx}\left(\frac{\partial f_B}{\partial(d\theta/dx)}\right)\delta\theta + \frac{\partial f_B}{\partial(d\theta/dx)}\frac{d}{dx}(\delta\theta), \tag{18}$$

thus, Eq. (17) can be written as

$$\delta f = \int_a^1 \left[\frac{\partial f_B}{\partial \theta} - \frac{d}{dx}\left(\frac{\partial f_B}{\partial(d\theta/dx)}\right)\right]\delta\theta dx$$
$$+ \left[\frac{d\Phi_S}{d\theta} + \frac{\partial f_B}{\partial(d\theta/dx)}\right]_{x=1}\delta[\theta(1)]$$
$$+ \left[\frac{d\Phi_S}{d\theta} - \frac{\partial f_B}{\partial(d\theta/dx)}\right]_{x=a}\delta[\theta(a)]. \tag{19}$$

From the condition for extrema $\delta f = 0$, we obtain the coefficients for each of the independent variations $\delta\theta$, $\delta\theta(1)$ and $\delta\theta(a)$ must vanish simultaneously. Therefore, f_B satisfies the Euler-Lagrange equation,

$$\frac{\partial f_B}{\partial \theta} - \frac{d}{dx}\left(\frac{\partial f_B}{\partial(d\theta/dx)}\right) = 0, \tag{20}$$

meanwhile, from the coefficients for $\delta\theta(1)$ and $\delta\theta(a)$, the weak anchoring conditions at the cylindrical surfaces are given as

$$\left.\frac{d\theta}{dx}\right|_{x=a} = \frac{\sigma_a \sin\theta(a)\cos\theta(a)}{\cos^2\theta(a) + \kappa \sin^2\theta(a)}, \tag{21}$$

$$\left.\frac{d\theta}{dx}\right|_{x=1} = -\frac{\sigma_1 \sin\theta(1)\cos\theta(1)}{\cos^2\theta(1) + \kappa \sin^2\theta(1)}. \tag{22}$$

For low frequencies excitations, by using the sum convention and by denoting $\partial_k \equiv \frac{\partial}{\partial x_k}$, thus the nematodynamic equation for the director is written in the following way:

$$\frac{dn_i}{dt} = W_{ik}n_k + \lambda(\delta_{il} - n_i n_l)A_{lk}n_k + \frac{1}{\gamma_1}(\delta_{ij} - n_i n_j)H_j, \tag{23}$$

where $\lambda = -\gamma_2/\gamma_1$ is a dimensionless parameter defined as the ratio of two viscosities,

$$H_j = \partial_j \pi_{ij} - \partial\mathcal{F}/\partial n_i, \quad \pi_{ij} = \frac{\partial\mathcal{F}}{\partial(\partial_j n_i)} \tag{24}$$

is the molecular field, and

$$A_{ij} = \tfrac{1}{2}(\partial_j v_i + \partial_i v_j), \tag{25}$$

$$W_{ij} = \tfrac{1}{2}(\partial_j v_i - \partial_i v_j) \tag{26}$$

are the rate of strain tensor and the vorticity tensor [32,33], respectively. Moreover, the dynamic equation for the velocity field is given as

$$\rho \frac{dv_i}{dt} = -\partial_i p + \partial_k \sigma_{ik}, \tag{27}$$

where ρ is the mass density, p is the pressure field and σ_{ij} is the stress tensor of the nematic which can be expressed as [32,37]

$$\sigma_{ij} = \alpha_1 n_i n_j n_k n_p A_{kp} + \alpha_2 N_i n_j + \alpha_3 n_i N_j + \alpha_4 A_{ij}$$
$$+ \alpha_5 n_j n_k A_{ik} + \alpha_6 n_i n_k A_{jk}, \tag{28}$$

with

$$N_i = \frac{dn_i}{dt} - W_{ij} n_j \tag{29}$$

and α_i the Leslie viscosities coefficients which satisfy the Parodi relation [33] $\alpha_2 + \alpha_3 = \alpha_6 - \alpha_5$. Also, in terms of these viscosities, $\gamma_1 = \alpha_3 - \alpha_2 \geqslant 0$, $\gamma_2 = \alpha_2 + \alpha_3$.

In the case of a Couette flow [38], Eqs. (23) and (27) take the form

$$0 = (\cos^2\theta + \kappa \sin^2\theta)\left(\frac{d^2\theta}{dx^2} + \frac{1}{x}\frac{d\theta}{dx}\right)$$
$$+ \frac{1}{2}(\kappa - 1)\sin(2\theta)\left(\frac{d\theta}{dx}\right)^2 + \frac{\kappa + q - 1}{2x^2}\sin(2\theta)$$
$$- \frac{R_2^2}{2K_1}(\gamma_1 + \gamma_2 \cos 2\theta)\left(x\frac{d\omega}{dx}\right) \tag{30}$$

and

$$0 = \frac{d}{dx}\left[\eta(\theta) x \frac{d\omega}{dx}\right] + 2\eta(\theta)\frac{d\omega}{dx}, \tag{31}$$

where

$$2\eta(\theta) = 2\alpha_1 \sin^2\theta \cos^2\theta + (\alpha_5 - \alpha_2)\sin^2\theta$$
$$+ (\alpha_6 + \alpha_3)\cos^2\theta + \alpha_4 \tag{32}$$

is the local viscosity of the nematic [32,39]. From the no-slip condition established by Eq. (3), the solution of Eq. (31) is found to be

$$\Delta\omega \equiv \omega(x) - \Omega_1 = \frac{bK_1}{R_2^2}\int_a^x \frac{ds}{s^3 \eta[\theta(s)]}, \tag{33}$$

where b is an integration constant given by the relation

$$\Delta\Omega \equiv \Omega_2 - \Omega_1 = \frac{bK_1}{R_2^2}\int_a^1 \frac{ds}{s^3 \eta[\theta(s)]}. \tag{34}$$

Therefore, from Eqs. (30), (31), and (33), the nonlinear differential equation satisfied by $\theta(x)$ is

$$0 = (\cos^2\theta + \kappa \sin^2\theta)\left(x^2 \frac{d^2\theta}{dx^2} + x \frac{d\theta}{dx}\right)$$
$$+ \frac{1}{2}(\kappa - 1)x^2 \sin(2\theta)\left(\frac{d\theta}{dx}\right)^2 + \frac{\kappa + q - 1}{2}\sin(2\theta)$$
$$- \frac{b}{2\eta(\theta)}(\gamma_1 + \gamma_2 \cos 2\theta). \tag{35}$$

The numerical solutions for Eq. (35) corresponding to the NLC 5CB were performed by using the shooting method [40,41] and are described in the next sections.

III. NLC DIRECTOR'S ORIENTATION, VELOCITY PROFILE AND FRÉEDERICKSZ TRANSITION

The parameters used in the numerical solutions are $K_1 = 1.2 \times 10^{-11}$ N, $K_3 = 1.5792 \times 10^{-11}$ N, $\alpha_1 = -0.0060$ Pa $-$ s, $\alpha_2 = -0.0812$ Pa $-$ s, $\alpha_3 = -0.0036$ Pa $-$ s, $\alpha_4 = 0.0652$ Pa $-$ s, $\alpha_5 = 0.0690$ Pa $-$ s, $\alpha_6 = -0.0208$ Pa $-$ s, $\gamma_1 = 0.0777$ Pa $-$ s, $\gamma_2 = -0.0848$ Pa $-$ s, $\epsilon_\perp = 6.6$ and $\epsilon_a = 13.15$ [32,42]. Furthermore, we consider that $T_{IN} - T = 10\,°C$ where $T_{IN} = 35\,°C$ is the clearing temperature at which 5CB suffers the transition from nematic to isotropic phase [43], and chosen dimensions of the cylinders such that $a = 0.5$.

Since the surfactant coating applied experimentally to each surface could be different in each of them, we define the ratio $\beta = \tau_{0_a}/\tau_{0_1}$. To show the effect of the surface anchoring energies on $\theta(x)$, numerical results are given by considering β and the effective surface anchoring energy σ_a [Eq. (16)].

We start by analyzing the case in which the surface anchoring energies τ_{0_a} and τ_{0_1} which amounts to set $\beta = 1$. In Figs. 2(a) and 2(b) we have depicted two sets of NLC configurations for the inclination angle of the director, $\theta(x)$, corresponding to $\sigma_a = 5$ and $\sigma_a = 15$, and parametrized by the value of q. In calculating numerically these textures, we have found that for each value of σ_a there is a threshold value q_c under which the NLC remains undistorted, that is $\theta(x) = 0$ for $q < q_c$. In other words, it was observed a configurational transition whose threshold value depends on the anchoring energy [30]. For the cases drawn in these plots, $q_c \sim 7.8$ for $\sigma_a = 5$ and $q_c \sim 13.3$ for $\sigma_a = 15$. Moreover, the threshold value q_c not only depends on σ_a, but also on the dimensionless parameter β as we will show below. Because for liquid crystal under different geometries and boundary conditions [9] the threshold q_c depends on the share rate, it is reasonable to ask this question. In the Appendix, we briefly show how for our model, the threshold does not depend on $\Delta\Omega$.

Also, it is observed that as σ_a increases, the intervals within the inclination angle at the cylindrical surfaces take values which are closer to zero and their thicknesses decrease; also, as the strength of the applied electric field increases, the values of θ decrease. This behavior is a consequence of the relation between the corresponding effective anchoring energies which for the case of the configurations of Fig. 2 satisfy $\sigma_a < \sigma_1$ for $\tau_{0_a} = \tau_{0_1}$.
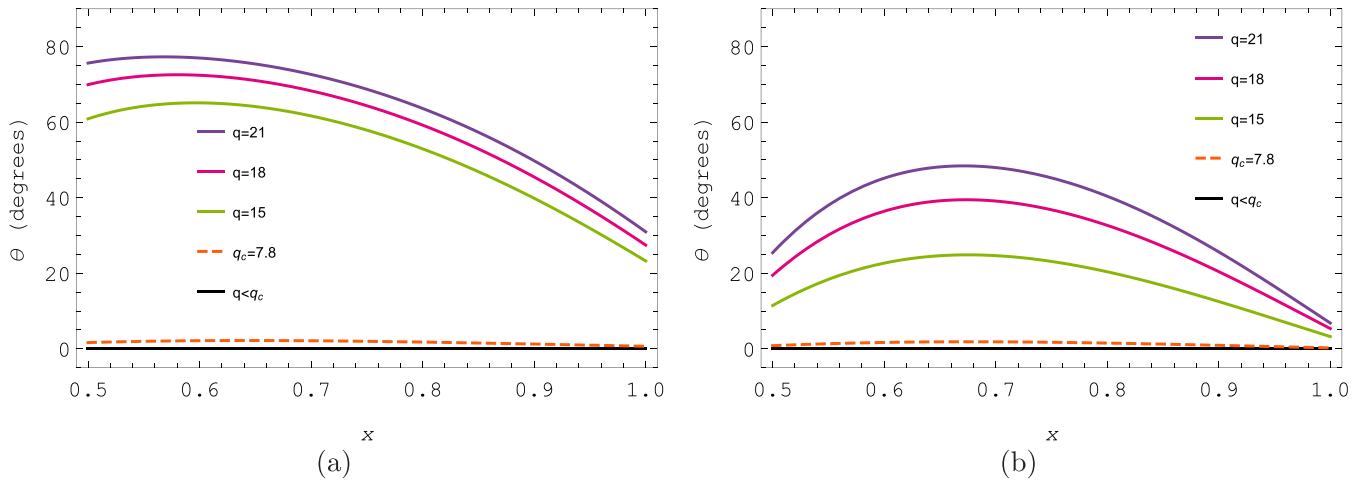
FIG. 2. Orientation of the NLC 5CB as a function of x. In panels (a) and (b), it is shown the plots for $\sigma_a = 5$ and $\sigma_a = 15$, respectively, and for different values of q. Dashed lines are the configurations at the Fréedericksz transition $q = q_c$ where $q_c \sim 7.8$ in panel (a) and $q_c \sim 13.3$ in panel (b).

Figures 3(a)– 3(c) show three sets of NLC configuration plots corresponding to $\beta < 1$, $\beta = 1$ and $\beta > 1$, respectively, and $\sigma_a = 10$. For $\beta \leqslant 1$ ($\sigma_a < \sigma_1$), as the strength of the applied electric field increases, it is observed that θ reaches a maximum whose value is closer to the inner cylinder while the director tends to get a parallel alignment at the outer
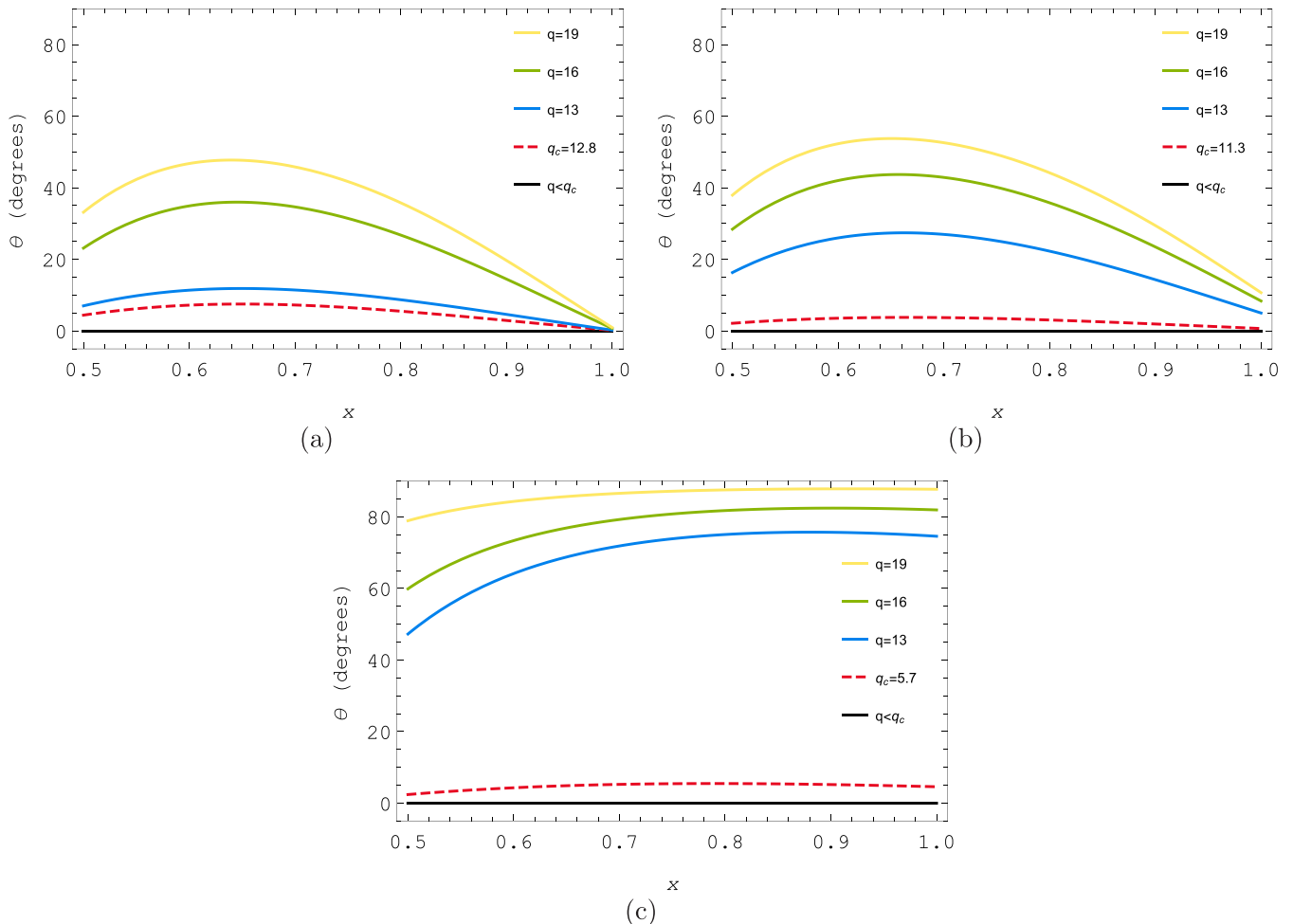

FIG. 3. Orientation of the NLC 5CB as a function of x. It is shown the plots for $\sigma_a = 10$ of the inclination angle $\theta(x)$ for q corresponding to $\beta = 0.1, 1, 10$ for panels (a), (b), and (c), respectively. For each value of β, q_c has a different value.
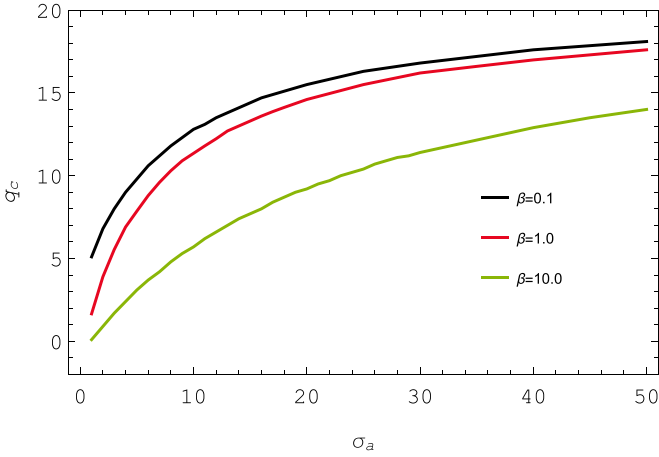
FIG. 4. Threshold field for the NLC 5CB as a function of σ_a for different values of $\beta = \tau_{0_a}/\tau_{0_1}$.

cylindrical surface [Figs. 3(a) and 3(b)]. For $\beta > 1$ ($\sigma_a > \sigma_1$) this maximum is closer to the outer cylinder, meanwhile the NLC molecules tend to align perpendicularly to this surface ($x = 1$), as it is observed in Fig. 3(c).

It is known that the Fréedericksz transition depends on the relation between the strength of the surface anchoring forces and that of the external electromagnetic force [30,33] which in our case correspond to σ_a and q, respectively. Therefore, for a given anchoring force at the cylindrical surfaces, the parameter q has to reach the critical value q_c to distort the molecules within the bulk. On the contrary, if $q < q_c$ the molecules of the nematic remain at the undistorted state which corresponds to $\theta(x) = 0$ for all $x \in (a, 1)$, as can be seen in Figs. 2(a) and 2(b).

In Fig. 4 it is shown the configurational transition threshold field q_c for $\beta = 0.1, 1, 10$. For each value of the parameter β, it is found that q_c is an increasing function of σ_a which tends asymptotically to $q_c \rightarrow 20.22$. This fact is in accordance to the result given by Reyes *et al.* [17], where electrorheological response of the present physical system with hard anchoring

conditions ($\sigma_a \rightarrow \infty$) is studied. Furthermore, for a given value of σ_a the corresponding threshold value increases as β decreases. In other words, from Eq. (16) and the definition of β, it can be observed that q_c increases or decreases depending on whether the effective anchoring energy at the outer cylinder (σ_1) is lesser or greater than the one at the inner cylinder (σ_a).

However, since both cylinders are rotating at different angular velocities and there is no relative motion between such surfaces along its symmetry axis, the NLC develops a Couette-Taylor flow. From every configuration of the nematic $\theta(x)$ the corresponding (angular) velocity profile is obtained from the numerical integration of Eq. (33). In Fig. 5(a) we have drawn the velocity profile for $q = 20$, $\sigma_a = 50$ and parametrized by $\Delta\Omega$, that is, each of the curves corresponds to the values $\Delta\Omega = 5 \text{ rad s}^{-1}$, 10 rad s^{-1}, 15 rad s^{-1}, 20 rad s^{-1}. It is found that the angular velocity of the nematic is a monotonically increasing function of x.

In Fig. 5(b) we considered specific values of the parameters σ_a and $\Delta\Omega$, namely, $\sigma_a = 50$ and $\Delta\Omega = 20 \text{ rad s}^{-1}$, to show velocity profiles for different values of q including the one corresponding to the threshold value at which the Fréedericksz transition takes place. It is observed that there is a common position $x_{50} \sim 0.72$ where the relative angular velocities have practically the same value. Moreover, this is a inflexion point where the curvature of every curve shown in this figure vanishes: $d^2\omega/dx^2 = 0$. To explain this, let us perform a direct calculation by using Eq. (33) which leads to the expression $(d\theta/dx)d\eta/d\theta = -3\eta/x$ for the inflexion point. Notice that because the effective viscosity defined in Eq. (32) is a monotonous function of the coordinate, the value of x satisfying this condition only depends on $d\theta/dx$. However, Figs. 2 and 3 exhibit that the maximum of $\theta(x)$ is almost independent of q, so the inflexion point of the $\Delta\omega$ curves as well. This means that roughly speaking the inflexion point of the angular velocity curve is controlled by the slope of the texture curve. Also, for $x \in [a, x_{50}]$ as the electric field strength increases, $\Delta\omega$ increases. Conversely, when $x \in [x_{50}, 1]$, we have the opposite behavior.
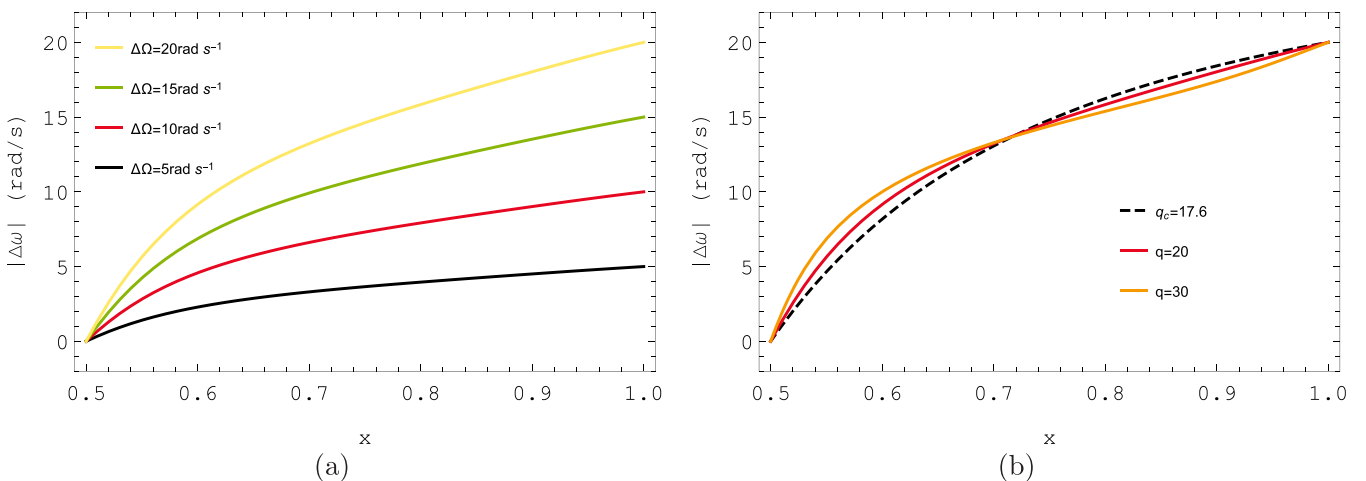

(a)

(b)

FIG. 5. (Angular) velocity profile $\Delta\omega$ as a function of x for the NLC 5CB. In panel (a) the values of the parameters q and σ_a are fixed at $q = 20$ and $\sigma_a = 50$. In panel (b) we show the plots of $\Delta\omega$ as a function of x for $\sigma_a = 50$, $\Delta\Omega = 20 \text{ rad s}^{-1}$ and different values of q, including the plot for $q_c \sim 17.6(\text{--})$.
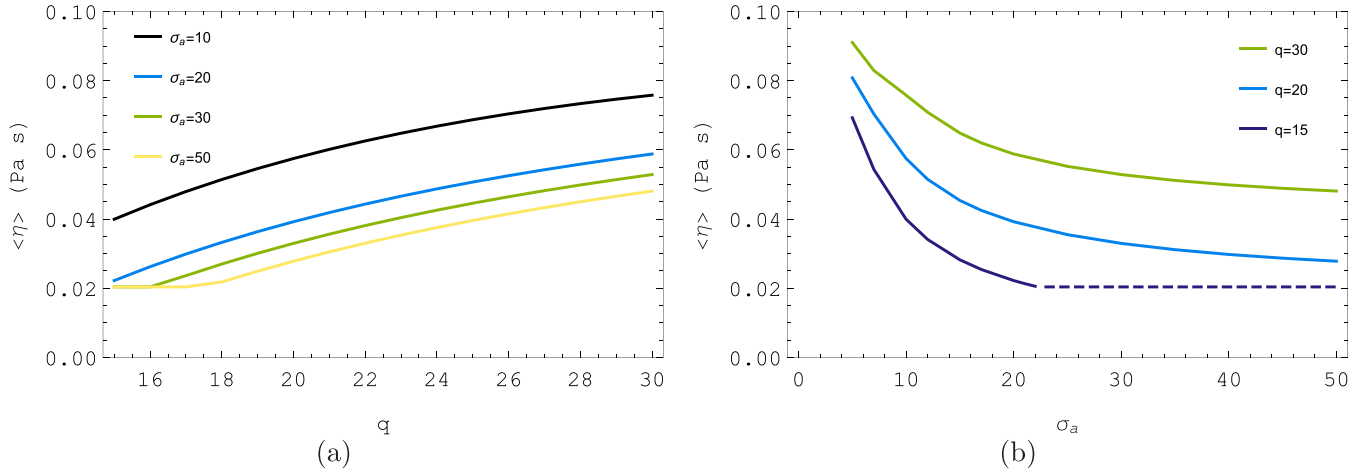
FIG. 6. Apparent viscosity $\langle\eta\rangle(q,\sigma_a)$ corresponding to the case $\beta=1$ and $\Delta\Omega = 20$ rad s^{-1}. In panel (a) we show $\langle\eta\rangle(q)$ as a function of q for different values of σ_a. In panel (b) we show $\langle\eta\rangle(\sigma_a)$ as a function of σ_a for different values of q; for the case $q=15$, dotted line corresponds to the viscosity for the NLC undistorted configuration.

IV. AVERAGED APPARENT VISCOSITY

Averaged apparent viscosity function $\langle\eta\rangle$ results from the integration of the local viscosity of the NLC $\eta(\theta)$ [Eq. (32)] over the cross section area of the flow. Considering the strong dependence of $\eta(x)$ on the external electric field and on the surface anchoring energy, thus

$$\langle\eta\rangle(q,\sigma_a) = \frac{2}{1-a^2}\int_a^1 \eta[\theta(x);q,\sigma_a]x\,dx, \qquad (36)$$

where we have indicated the dependence of $\eta[\theta(x)]$ on the dimensionless parameters q and σ_a. Electrorheological response of the NLC for $\Delta\Omega = 20$ rad s^{-1}, $\beta=1$ and different anchoring energies is shown in Fig. 6.

Figure 6(a) shows the apparent viscosity as a function of the parameter q for different values of σ_a and where we have considered that the coating applied anchoring energy at each cylindrical surface is the same ($\beta=1$). For a given value of σ_a, $\langle\eta\rangle$ exhibits a constant behavior for $q < q_c$ (where the NLC is in the undistorted state $\theta(x)=0$) which is clearly observed in the case $\sigma_a = 50$ where $q_c \sim 17.5$. Once the corresponding threshold value has been reached ($q \geqslant q_c$), it is found that $\langle\eta\rangle$ is an increasing function of q and the NLC is less viscous as σ_a increases [σ_a is the ratio between the effective surface anchoring energy at the inner cylinder and the elastic bulk energy, Eq. (16)], which is a consequence of the director orientation at the confined surfaces due to the effective anchoring forces. This behavior can also be observed in Fig. 6(b), where we plotted $\langle\eta\rangle$ as a function of σ_a for different values of q.

V. CONCLUDING REMARKS

We numerically obtained the configurations of an NLC with the physical properties of 5CB confined between two coaxial circular cylinders which rotate at different constant angular velocities, submitted to an external low-frequency radial electric field and where no-slip boundary conditions and weak anchoring conditions were considered. Instead of the surface anchoring energies τ_{0_a} and τ_{0_1}, we found that

electrorheological response of the NLC is based on the effective surface anchoring energies σ_a and σ_1 [Eq. (16)]. In addition to this, we introduced the parameter β to obtain the orientation of the director in the bulk for some values of the parameters $\Delta\Omega$, q and σ_a corresponding to the cases $\beta < 1$, $\beta = 1$, and $\beta > 1$.

From Fig. 2, it is observed that the intervals within the inclination angle of the director at the cylindrical surfaces takes values are narrower as σ_a increases. Furthermore, the orientation of the nematic molecules at the outer cylinder is highly dependent on whether $\beta \leqslant 1$ or $\beta > 1$ (Fig. 3). Also, for an increasing value of the electric field intensity, we obtained that the nematic at $x = 1$ tends to a parallel alignment for $\sigma_a < \sigma_1$ [Figs. 3(a) and 3(b)], meanwhile for the case $\sigma_a > \sigma_1$, $\theta(x)$ tends to a normal alignment [Fig. 3(c)].

It was observed that for each value of σ_a there is a Fréedericksz transition threshold field q_c which is an increasing function of σ_a and exhibits an asymptotic behavior as $\sigma_a \to \infty$ (Fig. 4). Moreover, q_c is related to the ratio of the effective surface anchoring energies (β) and its value decreases as the NLC molecules are stronger anchored at the outer cylinder than in the inner one.

The velocity profile of the nematic proved to be an increasing function of the parameters $\Delta\Omega$, q and σ_a (Fig. 5).

Since the director orientation at the cylinders tends to be parallel to such surfaces as the strength of the effective surface anchoring forces increases, the orientation of the molecules in the bulk tends to be more aligned to the flow of the nematic, which implies that the NLC has less viscosity (Fig. 6). However, because of the presence of the external electric field, NLC molecules are oriented along the radial direction, which is perpendicular to the nematic flow and causes an increase in the apparent viscosity.

APPENDIX

Here we shall study analytically the threshold for occurring the orientational transition. In the spirit of Ref. [10], for this purpose let us use the linearized version of Eqs. (34) and (35) around the undistorted configuration $\theta = 0$, which are given by

$$\Delta\Omega \equiv \Omega_2 - \Omega_1 = \frac{bK_1}{R_2^2} \int_a^1 \frac{ds}{s^3 \eta(\theta(s))}$$

$$= -\frac{bK_1}{2R_2^2 \eta(0)} \left(1 - \frac{1}{a^2}\right) + O(\theta^2) \quad \text{(A1)}$$

and

$$\left(x^2 \frac{d^2\theta}{dx^2} + x \frac{d\theta}{dx}\right) + (\kappa + q - 1)\theta$$

$$- \frac{b}{2\eta(0)}(\gamma_1 + \gamma_2) + O(\theta^2) = 0, \quad \text{(A2)}$$

respectively.

Solving Eq. (A1) for b and substituting in Eq. (A2), we get

$$\frac{d^2\theta}{d\varsigma^2} + (\kappa + q - 1)\theta + \frac{\Delta\Omega R_2^2 a^2}{K_1(a^2 - 1)}(\gamma_1 + \gamma_2) + O(\theta^2) = 0, \quad \text{(A3)}$$

where $\varsigma = \ln x$. The general solution for the last equation can be expressed as

$$\theta = A\cos(\varsigma\sqrt{\kappa + q - 1}) + B\sin(\varsigma\sqrt{\kappa + q - 1})$$

$$- \frac{\Delta\Omega R_2^2 a^2}{K_1(a^2 - 1)(\kappa + q - 1)}(\gamma_1 + \gamma_2), \quad \text{(A4)}$$

where A and B are constants to be determined by the linearized expressions of the boundary conditions given by Eqs. (21) and (22). Their explicit expressions are given by

$$A = \frac{a^2 \Delta\Omega R_2^2 \sigma_1(\gamma_1 + \gamma_2)}{\Xi}[a\sigma_a \cos(\sqrt{k+q-1}\ln a) + \sqrt{k+q-1}\sin(\sqrt{k+q-1}\ln a) - a\sigma_a], \quad \text{(A5)}$$

$$B = \frac{a^2 \Delta\Omega R_2^2(\gamma_1 + \gamma_2)}{\Xi}[a\sigma_a(\sqrt{k+q-1} - \sigma_1 \sin(\sqrt{k+q-1}\ln a)) + \sigma_1\sqrt{k+q-1}\cos(\sqrt{k+q-1}\ln a)], \quad \text{(A6)}$$

where

$$\Xi = K_1(a^2-1)(k+q-1)[(k+q-1-a\sigma_1\sigma_a)\sin(\sqrt{k+q-1}\ln a) + \sqrt{k+q-1}(a\sigma_a+\sigma_1)\cos(\sqrt{k+q-1}\ln a)]. \quad \text{(A7)}$$

The condition for this solution to be physically acceptable is that $\Xi > 0$ because for $\Xi = 0$ the solution is divergent and for $\Xi < 0$, it is a nonphysical reorientation angle provided by a complex valued solution. It is straightforward to check that the same condition is hold for a vanishing flow ($\Delta\Omega = 0$). Indeed, the threshold value for q given by the condition $\Xi = 0$ is independent of the value of $\Delta\Omega$.

[1] F. Reinitzer, Beiträge zur Kenntniss des Cholesterins, Monatschefte für Chemie **9**, 421 (1888).

[2] B. Bahadur, *Liquid Crystals: Applications and Uses* (World Scientific, Singapore, 1990).

[3] D. Demus, J. Goodby, G. W. Gray, H.-W. Spiess, and V. Vill, *Handbook of Liquid Crystals* (Wiley-VCH, Germany, 1998).

[4] M. C. Parker, Dynamics holograms for wavelength division tiplexing, Ph.D. thesis, University of Cambridge, 1996.

[5] M. Parsley, *The Hallcrest Handbook of Thermochromic Liquid Crystals Technology* (Hallcrest, Glenview, 1991).

[6] J. Atkin and F. M. Leslie, Couette flow of nematic liquid crystals, in *The Quarterly Journal of Mechanics and Applied Mathematics* (Oxford University Press, Oxford, 1970), Vol. 23, Issue 2, pp. 3–24.

[7] D. R. M. Williams and A. Halperin, Nematic liquid crystal in a tube: The Fréeedericksz transition, Phys. Rev. E **48**, R2366 (1993).

[8] I. V. Kotov, M. V. Khazimullin, and A. P. Krekhova, Flexoelectric instability in nematic liquid crystal between coaxial cylinders, Mol. Cryst. Liq. Cryst. **366**, 2737 (2001).

[9] H. Tsuru, Stability analysis of nematics between two concentric cylinders, J. Phys. Soc. Jpn. **59**, 1600 (1990).

[10] P. G. de Gennes and J. Prost, *The Physics of Liquid Crystals*, (Pergamon, Oxford, 1993).

[11] D. R. M. Williams, Nematic liquid crystals between antagonistic cylinders: Spirals with bend-splay director undulations, Phys. Rev. E **50**, 1686 (1994).

[12] R. Rosso, E. G. Virga, and S. Kralj, Elastic actions exchanged by eccentric cylinders in liquid crystals, Phys. Rev. E **74**, 061703 (2006).

[13] S. U. Ilyas, R. Pendyala, and N. Marneni, Preparation, sedimentation, and agglomeration of nanofluids, Chem. Eng. Technol. **37**, 2011 (2014).

[14] M. De Volder, K. Yoshida, S. Sokota, and D. Reynaerts, The use of liquid crystals as electrorheological fluids in microsystems:model and measurements, J. Micromechanics Microengineering **16**, 612 (2006).

[15] K. Yoshida, M. Kikuchi, J. H. Park, and S. Yokota, Fabrication of micro electro-rheological valves (er valves) by micromachining and experiments, Sens. Actuat. A: Phys. **95**, 227 (2002).

[16] I. Yang and A. D. Shine, Electrorheology of a nematic poly(n-hexyl isocyanate) solution, J. Rheol. **36**, 1079 (1992).

[17] J. A. Reyes, A. Corella-Madueño, and C. I. Mendoza, Electrorheological response and orientational bistability of a homogeneously aligned nematic capillary, J. Chem. Phys. **129**, 084710 (2008).

[18] D. Martínez and J. A. Reyes, The role of the anchoring conditions in electrorheological behavior of a nematic constrained

by two coaxial cylinders and submitted by a pressure drop, Liq. Crys. **44**, 996 (2017).

[19] J. A. Castellano, Surface anchoring of liquid crystal molecules on various substrates, Mol. Crys. Liq. Crys. **94**, 33 (1983).

[20] K. Takatoh, M. Hasegawa, M. Koden, N. Itoh, R. Hasegawa, and M. Sakamoto, *Alignment Technologies and Applications of Liquid Crystals Devices* (Taylor & Francis, New York, 2005).

[21] M. Rüetschi, P. Grütter, J. Fünfschilling, and H. Güntherodt, Creation of liquid crystal waveguides with scanning force microscopy, Science **265**, 512 (1994).

[22] A. J. Pidduck, S. D. Haslam, G. P. Bryan-Brown, R. Bannisterand, and I. D. Kitely, Control of liquid crystal alignment by polyimide surface modification using atomic force microscopy, Appl. Phys. Lett. **71**, 2907 (1997).

[23] W. M. Gibbons, P. J. Shannon, S. Sun, and B. J. Swtlin, Surface-mediated alignment of nematic liquid crystals with polarized laser light, Nature **351**, 49 (1991).

[24] V. G. Chigrinov, V. M. Kozenkov, and H.-S. Kwok, *Photoalignment of Liquid Crystalline Materials: Physics and Applications* (John Wiley & Sons, London, 2008).

[25] A. Rapini and M. Papoular, Distorsion d'une lamelle nématique sous champ magnétique conditions d'ancrage aux parois, J. Physique Colloq. **30**, C454 (1969).

[26] M. Rahimi, T. F. Roberts, J. C. Armas-Perez, X. Wang, E. Bukusoglu, N. L. Abbott, and J. J. de Pablo, Nanoparticle self-assembly at the interface of liquid crystal droplets, Proc. Natl. Acad. Sci. U.S.A. **112**, 5297 (2015).

[27] O. Lavrentovich, B. Lev, and A. Trokhymchuk, Foreword: Liquid crystal colloids, Condens. Matter Phys. **13**, 30101 (2010).

[28] V. Fréedericksz and V. Zolina, Forces causing the orientation of an anisotropic liquid, Trans. Faraday Soc. **29**, 919 (1933).

[29] V. Fréedericksz and V. Zwetkoff, Über die Orientierung der anisotropen Flüssigkeiten in dünnen Schichten und die Messung einiger ihre elastischen Eigenschaften charakterisierenden Konstanten, Phys. Z. Sowjetunion **6**, 490 (1934).

[30] P. G. De Genes and J. Prost, *The Physics of Liquid Crystals* (Clarendon Press, New York, 1993).

[31] C. H. Chen RH, *Liquid Crystal Displays: Fundamental Physics and Technology* (Wiley & Sons, New York, 2011).

[32] I. W. Stewart, *The Static and Dynamic Continuum Theory of Liquid Crystals* (Taylor & Francis, London, 2004).

[33] M. Kleman and O. D. Lavrentovich, *Soft Matter Physics: An Introduction* (Springer-Verlag, New York, 2003).

[34] G. Barbero and L. R. Evangelista, *Adsortion Phenomena and Anchoring Energy in Nematic Liquid Crystals* (Taylor & Francis, New York, 2006).

[35] G. P. Crawford, D. W. Allender, and J. W. Doane, Surface elastic and molecular-anchoring properties of nematic liquid crystals confined to cylindrical cavities, Phys. Rev. A **45**, 8693 (1992).

[36] L. M. Blinov and V. G. Chigrinov, *Electrooptic Effects in Liquid Crystal Materials* (Springer-Verlag, New York, 1994).

[37] L. D. Landau and E. M. Lifshitz, *Fluid Mechanics* (Pergamon, Oxford, 2003).

[38] P. K. Currie, Couette flow of a nematic liquid crystal in the presence of a magnetic field, Arch. Rat. Mech. Anal. **32**, 222 (1970).

[39] T. Carlsson, Theoretical Investigation of the shear flow of nematic liquid crystals with the Leslie viscosity $\alpha_3 > 0$: Hydrodynamic analogue of first-order phase transitions, Mol. Cryst. Liq. Cryst. **104**, 307 (1984).

[40] M. R. Osborne, On shooting methods for boundary value problems, J. Math. Anal. Appl. **27**, 417 (1969).

[41] W. H. Press, S. A. Teukolsky, W. T. Vetterling, and B. P. Flannery, *Numerical Recipes: The Art of Scientific Computing* (Cambridge University Press, New York, 2007).

[42] A. Bogi and S. Faetti, Elastic, dielectric and optical constants of 4-n-pentyl-4-cyanobiphenyl, Liq. Crys. **28**, 729 (2001).

[43] J. A. Reyes, J. A. Reyes-Avendaño and P. Halevi, Electrical tuning of photonic crystals infilled with liquid crystals, Opt. Commun. **28**, 2535 (2008).